Polymer 51 (2010) 5525–5531

Contents lists available at ScienceDirect

Polymer

journal homepage: www.elsevier.com/locate/polymer

Polypropylene-graphite nanocomposites made by solid-state shear pulverization: Effects of significantly exfoliated, unmodified graphite content on physical, mechanical and electrical properties

Katsuyuki Wakabayashi [a,1], Philip J. Brunner [a], Jun'ichi Masuda [a,2], Sheldon A. Hewlett [b], John M. Torkelson [a,b,*]

[a] Department of Chemical and Biological Engineering, Northwestern University, Evanston, IL 60208, USA
[b] Department of Materials Science and Engineering, Northwestern University, Evanston, IL 60208, USA

ARTICLE INFO

Article history:
Received 25 June 2010
Received in revised form
30 August 2010
Accepted 3 September 2010
Available online 15 September 2010

Keywords:
Nanocomposites
Graphite
Pulverization

ABSTRACT

Nanocomposites made from polypropylene and as-received graphite were prepared by solid-state shear pulverization (SSSP) as a function of graphite loading (0.3–8.4 wt%). X-ray diffraction indicates that SSSP employing harsh pulverization conditions yields substantial graphite exfoliation at 0.3–2.7 wt% graphite content with less exfoliation being achieved at higher graphite content. With increasing graphite content, thermal degradation temperature and non-isothermal onset crystallization temperature increase substantially (by as much as 35 and 23 °C relative to neat polypropylene) while isothermal crystallization half-time decreases dramatically. In contrast, Young's modulus and tensile yield strength exhibit maxima (~100% and ~60% increases, respectively, relative to neat polypropylene) at 2.7 wt% graphite content, with all nanocomposites retaining high elongation at break values except at the highest filler loading. Electrical conductivity measurements indicate percolation of graphite at 2.7 wt% and higher graphite content, consistent with rheology measurements showing the presence of a solid-like response of melt-state shear storage modulus as a function of frequency. Significant tunability of graphite exfoliation and property enhancements is demonstrated as a function of SSSP processing.

1. Introduction

Polymer nanocomposites are of major scientific and technological interest because of the potential to achieve enhanced material performance compared to neat polymer or conventional microcomposites [1–55]. Ideally, with nanocomposites, a small quantity of filler particles having a nano-length scale in at least one dimension is dispersed in a polymer matrix. Under such circumstances, the intrinsic properties of the nanofiller as well as the significant polymer–nanofiller interfacial interactions altering the properties of the polymer matrix [8–10] have the potential to result in outstanding improvements in material properties, ranging from mechanical and thermal robustness to thermal and electrical conductivity, depending on the choice of nanofiller. Many nanofillers can be considered for nanocomposite fabrication and property enhancements, although layered silicates [1–4,6,12–15], such as montmorillonite and bentonite, naturally available as clay, and carbon nanotubes [10,16–28,55], requiring chemical synthesis, have been among the most heavily studied and reported. With both layered silicates and carbon nanotubes, property enhancements are strong functions of exfoliation and/or dispersion of the nanofiller. With few exceptions [12], high levels of exfoliation and/or dispersion are generally very difficult to achieve using industrially scalable approaches for mixing unmodified polymer and unmodified nanofiller [56].

Over the past five years, there has been a renaissance in the study of graphite, resulting in it becoming a nanomaterial of choice for nanocomposite production. Bulk graphite [57,58] can be exfoliated into individual sp^2-hybridized carbon layers (termed graphene sheets) [59–65], which exhibit a combination of exceptional physical properties, including Young's modulus of ~1 TPa [57] and thermal conductivity of $\sim 5 \times 10^3$ W m^{-1} K^{-1} [64]. When appropriately incorporated into a polymer matrix, graphite has the potential to be an excellent nanofiller, as the graphene chemical structure is identical to that of carbon nanotubes and its stacked sheet morphology is analogous to that of layered silicates.

* Corresponding author. Department of Chemical and Biological Engineering, Northwestern University, Evanston, IL 60208, US. Tel.: +1 847 491 7449; fax: +1 847 491 3728.
E-mail address: j-torkelson@northwestern.edu (J.M. Torkelson).
[1] Present address: Department of Chemical Engineering, Bucknell University, Lewisburg, PA 17837, USA
[2] Present address: Films & Film Products Research Laboratories, Toray Industries, Inc., Otsu, Shiga 520-8558, Japan

0032-3861/$ – see front matter © 2010 Published by Elsevier Ltd.
doi:10.1016/j.polymer.2010.09.007

However, as made evident by reports on polymer (nano-) composites made with graphite or graphene [29–55], exfoliation and dispersion of nanoscale graphite layers and graphene sheets in polymers are extremely difficult to achieve using conventional, industrially scalable processing techniques and unmodified materials. These challenges may be even greater than those present with layered silicates, because the typical interlayer spacing in unmodified clay is ~1 nm while the interlayer spacing of graphene sheets in unmodified graphite is 0.335 nm [58]. The vast majority of previous reports of polymer-graphite nanocomposites exhibiting some improvement in properties relative to neat polymer involve graphite that has been pretreated by heat, acid and other intercalating chemicals, and/or sonication and microwave radiation, resulting in modified fillers [29–40,42–44,46,47,49,51–55] termed expandable/expanded graphite, exfoliated graphite, exfoliated graphite nanoplatelets, exfoliated graphite/graphene oxide, or functionalized graphite/graphene sheets. However, even with filler pretreatment and/or interfacial compatibilization, nanocomposite fabrication by conventional melt processing techniques often leads to (re)-aggregated morphology and/or only modest property improvement.

Recently, an industrially scalable processing method called solid-state shear pulverization (SSSP) was shown to yield fine nanoscale dispersion and substantial exfoliation of 2.5 wt% unmodified, as-received graphite in polypropylene (PP) [50]. The SSSP process, which has also been applied to achieve in situ compatibilization of immiscible polymer blends [66,67], nanoscale blends [68], exfoliation of clay [69] and debundling and dispersion of carbon nanotubes [24–26] in polymer nanocomposites, exposes the materials being processed near room temperature to high shear and compressive forces leading to absorption of energy. When sufficient energy is absorbed, the material will fracture and fragment at its weakest location, which may lead to delamination or exfoliation of filler consisting of layered sheets such as clay or graphite. Here we present the results of the first study of the effect of graphite content on a broad range of properties, including thermal, electrical, rheological and mechanical, exhibited by polymer nanocomposites made by SSSP. We also demonstrate the strong effect of SSSP process conditions on selected properties of the resulting nanocomposites.

2. Experimental section

2.1. Materials

Polypropylene was obtained from Total Petrochemicals (Atofina PP-3277, MFI = 1.8 g/10 min at 230 °C) and used as received. Unmodified, as-received graphite was provided by Asbury Carbon (average flake diameter = 2 μm, surface area = 113 m^2/g), and used without pretreatment. No solvents, modifiers, compatibilizers, or processing aids were used.

2.2. Preparation of nanocomposites by SSSP

Polypropylene pellets and varying amounts of graphite particles (0, 0.3, 1.0, 3.0, 5.0, and 10.0 wt% nominal) were manually dry-blended in a container prior to being co-fed by a K-Tron Soder S-60 feeder into the Berstorff ZE-25P SSSP instrument. The SSSP apparatus is a modified twin-screw extruder with 25-mm diameter barrels and length to diameter ratio of 26.5. Unlike a conventional twin-screw melt extruder, the process occurs within cooled barrels maintained well below room temperature (by a −7 °C ethylene glycol-water mixture as the cooling medium) and in two distinct processing regions along the pulverizer screw. The mixing region involving conventional bilobe screw elements causes intimate mixing between the filler and the polymer and coarse-grinds the material, while the subsequent pulverization region with trilobe screw elements further imparts high levels of shear and compressive stresses, resulting in repeated fragmentation and fusion of the material. Refs. [66–68] and [70] provide details on the SSSP process and equipment. For this study, nanocomposites were processed with a screw design involving two forward, three neutral, and one reverse mixing elements and three forward, two neutral and two reverse pulverization elements; the pulverization zone was setup with narrower, 23-mm diameter barrels. Unless otherwise noted, the material was processed through the SSSP instrument five times (5-pass), which is considered a harsh processing condition compared to the 1-pass processing case. A material feed rate of ~100 g/h and a screw speed of 300 rpm were employed, which resulted in fine, uniformly black, powder output.

2.3. Characterization

A Mettler-Toledo 851e thermogravimetric analyzer (TGA) and an 822e differential scanning calorimeter (DSC) were used for thermal characterization. A standard 10 °C/min heating ramp was employed in the TGA to monitor thermal degradation behavior under a nitrogen atomosphere and to determine the actual graphite content of the nanocomposites. Using a non-isothermal 10 °C/min cooling ramp, the onset crystallization temperature was measured via DSC. Isothermal DSC measurements were also made, which involved maintaining the specimen at 148 °C for 180 min after quenching from the melt state and recording the heat flow as a function of time; the crystallization half-time was determined from the integrated heat flow as a function of time. Percent PP crystallinity was evaluated by dividing the integrated area under the DSC 10 °C/min heating curve of a sample isothermally crystallized at 148 °C for a minimum of 180 min by the PP mass fraction to calculate the heat of fusion (ΔH_f) of PP in the sample; this value was subsequently divided by the theoretical ΔH^o_f of 100% PP of 207.1 J/g [71].

For mechanical property measurements, extreme care was taken in consistent preparation of test specimens, as thermal history and/or inconsistent exposure to high temperature may affect crystallinity and in turn physical properties of polyolefins. Upon pressing the polymer or nanocomposite sample in a brass compression mold set in a PHI hot press at 210 °C for 5 min, the mold assembly was transferred to a PHI cold press at 16 °C and held for 5 min. The cooled specimen was then removed and stored at room temperature for 12 h prior to being tested. Tensile test specimens were prepared according to ASTM D1708; films of ~0.5 mm in thickness were molded, and dumbbell-shaped specimens were cut out using a calibrated Dewes-Gumbs die. An MTS Sintech 20/G tensile tester, equipped with a 100 kN load cell, was operated at a crosshead speed of 5 cm/min for Young's modulus, elongation at break, and yield strength measurements. Impact strength was measured using Tinius-Olsen IT504 pendulum tester, in an unnotched Izod setup according to ASTM D4812; molded rectangular specimens of 60.1 mm in length, 12.6 mm in width, and 3.4 mm in height were used.

Rheological characterization was conducted using a TA Instruments ARES rheometer with 25-mm parallel-plate fixtures. A dynamic frequency sweep from 0.01 to 100 rad/s was employed and the material was maintained in a nitrogen atmosphere at 200.0 °C.

Electrical conductivity was evaluated on broken impact test specimens, where the measurements were made across the width of the slab. Although conductivity measurements are typically made across thin sheets, often with surfaces polished, sanded or etched, we have found that thinly pressed samples exhibited

substantial orientation of nanofillers which strongly impacted the measured conductivity; in contrast, the as-molded impact bars allowed for nanofillers to be more isotropically oriented and reflected true conductivity and the percolation threshold in isotropically oriented nanocomposites. Copper strips of 40 mm × 3.4 mm × 0.1 mm dimension were used as electrodes, and liquid silver (PELCO Colloidal Silver) was applied between the specimen and the electrodes to ensure full electrical contact. The sample assembly, sandwiched between two PMMA slabs and held in place by screws, was subjected to a room-temperature frequency sweep from 10^{-2}–10^{7} Hz with 0.1 V AC in a Solartron 1260 impedance spectrometer, from which conductivity values (κ) were calculated from the real component of measured impedance.

X-ray diffraction (XRD) was performed on a Rigaku ATX-G, operating with a Cu Kα radiation at 50 kV and 240 mA, on 1.6 mm-thick melt-molded disc specimens; the goniometer was set at the rate of 1°/min and scan width of 0.05°.

3. Results and discussion

3.1. Nanocomposite composition and X-ray diffraction data

Table 1 lists the PP-graphite series under investigation, with actual graphite contents determined at a common reference temperature of 550 °C from TGA profiles. (Neat PP is fully degraded and volatilized at 550 °C while graphite is fully stable at this temperature). The actual filler percentages of the nanocomposites obtained as SSSP output are slightly lower than the nominal values related to SSSP input of graphite powder relative to PP pellet. This is explained by the fact that small levels of the graphite powder stick to the metallic surfaces of the hopper, screws, and barrels during nanocomposite fabrication. For the remainder of the discussion, the nanocomposite samples are denoted as "PP-xG" where x denotes w_{act} (actual graphite content) in wt%.

Fig. 1 shows XRD data of the PP-G series processed by SSSP under harsh processing conditions as well as those of neat PP and neat graphite. For neat polymer and all polymer nanocomposite samples, the specimen preparation method was consistent to ensure comparable specimen dimensions and filler orientation. The linear-scale X-ray intensity for the PP-G samples was normalized by making the total area under all PP crystal peaks in the nanocomposites equal. (Crystallinity levels in the PP-G samples were identical within error as determined by DSC measurements). First-order confirmation of normalized PP-G XRD curves (b)–(f) in Fig. 1 is the characteristic PP (060) crystalline peak at $2\theta \approx 25.3°$ being of equivalent magnitude. The XRD curve of pure graphite powder, was acquired using a conventional powder mount, and was scaled to fit in the figure. The graphite characteristic peak occurs at $2\theta \approx 26.3°$, corresponding to the inter-graphene sheet spacing of 0.338 nm according to Bragg's law. These values are comparable to the accepted value of 0.335 nm in graphite crystallography [58].

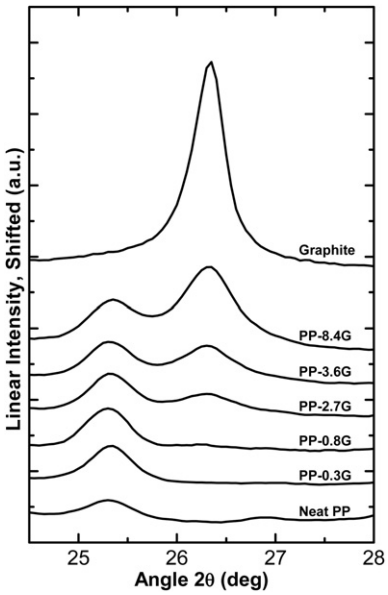

Fig. 1. X-ray diffraction of neat PP pellet, pure graphite powder, and PP-graphite nanocomposite series. Intensities of nanocomposite samples have been normalized by making the total area under all PP crystal peaks (most peaks not shown) equal. (Crystallinity levels of the PP in the nanocomposites were identical at determined by DSC measurements).

Comparison of the XRD data as a function of graphite composition reveals a general trend of increasing graphene peak height (and ratio of graphene peak height to PP (060) crystalline peak height) with filler loading, which is expected simply because of the absolute content of graphite particles. The low-loading samples (PP-0.3G and PP-0.8G) show virtually no visible graphite peak at $2\theta \approx 26.3°$. It should be noted that the most highly loaded PP-8.4G sample shows a comparable ratio of the PP (060) crystalline peak height to the graphene peak height as a melt-processed 2.8 wt% graphite PP composite [50]. This result signifies that the extent of graphite platelet layering in the SSSP-processed 8.4 wt% graphite nanocomposite is comparable to that of melt-mixed 2.8 wt% graphite composite, which had little to no graphite exfoliation. These results indicate that SSSP processing can lead to significant exfoliation of graphite nanoplatelets in PP for a wide range of graphite loadings, albeit with a decrease in the fraction of graphite being in the exfoliated state with increasing graphite content as characterized by XRD.

3.2. Thermal properties

Exfoliated and dispersed graphite nanoplatelets in the PP matrix are expected to influence physical properties of the resulting

Table 1
Thermal Property Measurements in PP-Graphite Nanocomposite Samples.

Samples	Actual Graphite Content w_{act} (wt%)	Non-isothermal Onset Crystallization Temperature T_c (°C)	Isothermal Crystallization Half-Time, at 148 °C $\tau_{1/2}$ (min)	Percent PP Crystallinity[a] Xc (%)	Thermal Degradation Temperature, at 5 wt% Loss of Total Mass T_{deg} (°C)
Neat PP, Pellet	0	117	–[b]	–[b]	403
PP-0.3G	0.27	131	46	50.3	416
PP-0.8G	0.81	135	33	50.7	418
PP-2.7G	2.7	138	23	50.8	430
PP-3.6G	3.6	139	16	50.3	435
PP-8.4G	8.4	140	12	50.8	438

[a] Crystallinity was measured upon heating after 180 min of isothermal hold at 148 °C.
[b] No crystallization was observed after 180 min.

nanocomposites. Table 1 summarizes how graphite content affects crystallization kinetics in the SSSP-processed samples. Compared with neat PP, the non-isothermal crystallization onset temperature (T_c), measured at a 10 °C/min cooling rate, is 14–23 °C higher in the nanocomposites, with a monotonic increase in T_c observed with graphite content. Fig. 2a compares the non-isothermal crystallization curves as measured by DSC. An increase in graphite loading leads to wider, shallower exothermic curves with higher onset and end crystallization temperatures; this indicates that the dispersed graphite nanoplatelets not only act as seeds for faster nucleation but also as barriers to the formation of large polypropylene crystallites.

A temperature of 148 °C was selected to allow for precise determination of isothermal crystallization half-times ($\tau_{1/2}$) in the PP nanocomposites. Fig. 2b shows the DSC traces associated with these measurements, with the resulting $\tau_{1/2}$ values listed in Table 1. At this temperature, $\tau_{1/2}$ ranges from 46 min for PP-0.3G to 12 min for the PP-8.4G. The extent to which the graphite nanoplatelets serve as effective nucleation sites for crystallization is made clear by the fact that neat PP exhibits no crystallization after 180 min at 148 °C. Isothermal crystallization measurements on neat PP conducted at a much lower temperature of 135 °C result in a $\tau_{1/2}$ of 59 min, which is larger than any of the $\tau_{1/2}$ values measured in the PP-graphite nanocomposites at 148 °C. These results demonstrate that the graphite nanoplatelets serve as tremendously effective nucleating agents for the crystallization of PP.

It is also noteworthy that the shapes of the isothermal crystallization curves in Fig. 2b differ between lower and higher graphite content nanocomposites. The samples with 0.3 and 0.8 wt% graphite content exhibit highly symmetric, somewhat S-shaped crystallization curves. In contrast, the samples with higher graphite content rise more sharply at low crystallinity levels but have lower slopes at higher crystallinity levels. These results are consistent with the non-isothermal crystallization behavior and the fact that graphite nanoplatelets serve both as highly effective nucleation sites and as barriers for growth of crystals.

The level of PP crystallinity in the nanocomposites, as measured upon heating through the melt transition following the 148 °C isothermal crystallization, was 50–51%, independent of graphite content. (See Table 1). This crystallinity level is only slightly higher than that obtained for neat PP (45%, measured upon heating for a sample that had been cooled to room temperature). Similar behavior has been reported in other semicrystalline polymer-based hybrids [14,24] in which the neat polymer is highly crystallizable.

Fig. 3 compares thermogravimetric analysis data of neat PP, neat graphite, and the PP nanocomposites as a function of graphite content. The normalized sample mass is based on the original mass at room temperature and thus is slightly less than 1.00 at 360 °C (even for neat graphite) because of the loss of moisture and organic impurities in the specimens. Graphite is shown to be extremely thermally stable over a temperature range of 360–460 °C. In contrast, neat PP exhibits a greater than 15% mass degradation and volatilization upon heating in a nitrogen atmosphere over the temperature range of 360–430 °C. The thermal degradation curves of the nanocomposite series fall between those of neat PP and pure graphite, with the curves gradually shifting outward from the neat PP curve with increasing graphite content.

Table 1 reports thermal degradation temperature (T_{deg}), which is defined here as temperature at 5 wt% loss, for the PP-graphite series. There are large increases of T_{deg} with increasing graphite content—by 27 °C with 2.7 wt% graphite and 35 °C with 8.4 wt% graphite. This general behavior originates from the filler particles acting as thermal and transport barriers in the polymer matrix. We note that care should be taken in drawing comparisons of the increases in T_{deg} with those reported in other studies of PP nanocomposites. This arises from three factors: (1) the different temperature ramp rates that are employed, (2) the different manners in which T_{deg} may be defined based on mass loss, and (3) the fact that T_{deg} is usually a function of any organic modification of the nanofiller.

3.3. Electrical conductivity and rheology

In contrast to many nanofillers, carbon-based nanofillers such as graphite have the potential to yield an electrically conductive

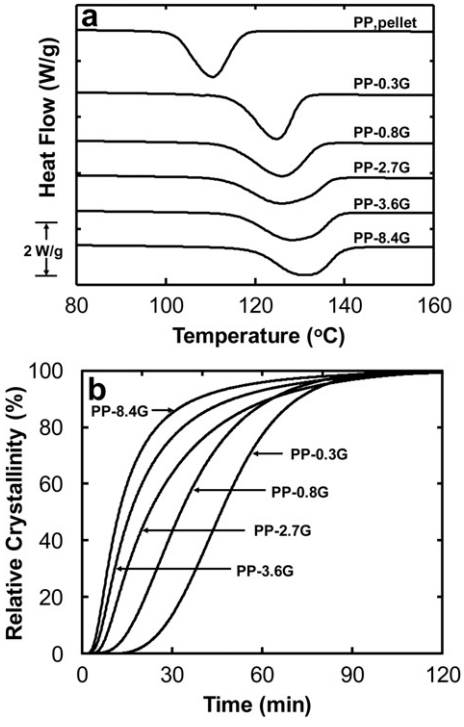

Fig. 2. (a) Non-isothermal (10 °C/min) and (b) isothermal crystallization (148 °C) curves for neat PP pellet and PP-graphite nanocomposites. Note that the isothermal curve for neat PP pellet is not available because the sample did not develop any significant level of crystallinity.

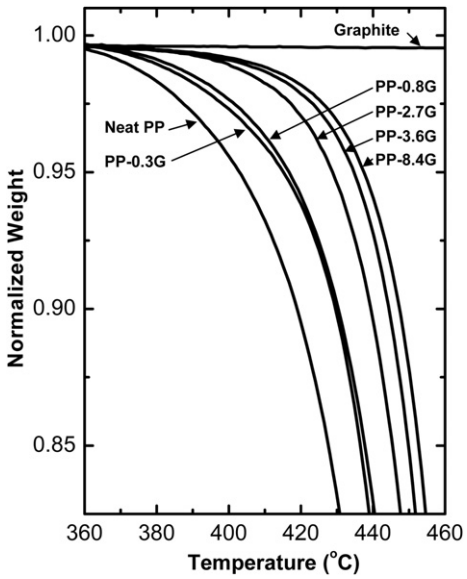

Fig. 3. TGA curves of neat PP, pure graphite powder, and PP-graphite nanocomposites in the region of onset thermal degradation (nitrogen atmosphere with a heating rate of 10 °C/min).

nanocomposite. Electrical conductivity correlates with the "connectivity" of the carbon-based filler particles, which is necessary to provide a pathway for electrical conduction across the samples. At low nanofiller content, a potential prerequisite for achieving electrical conduction is exfoliation and dispersion of the graphite nanoplatelets, with an additional prerequisite being that the dispersion allows for the presence of a network-like structure of the nanofiller across the sample. Electrical conductivity data of the nanocomposites, as determined by impedance spectroscopy measurements, are presented in Fig. 4. Neat PP and PP-0.3G exhibited virtually zero conductivity, and thus their data points are missing from Fig. 4. In contrast, PP-0.8G exhibited an electrical conductivity on the order of 10^{-9} S/cm while the higher graphite content nanocomposites exhibited electrical conductivity on the order of 10^{-4} to 10^{-3} S/cm. These results indicate that a percolation threshold is achieved in these SSSP-processed samples between 0.8 and 2.7 wt% (0.3 and 1.1 vol%) graphite content. This is the lowest percolation threshold achieved in polymer nanocomposites with unmodified, as-received graphite. The relatively modest level of electrical conductivity achieved in the percolated samples is likely associated with the fact that the as-received graphite used in this study has a reported neat-state electrical conductivity of 6–7 S/cm. If graphite with higher electrical conductivity was employed, it is likely that the achievable electrical conductivity in the SSSP-processed samples would scale with the electrical conductivity of the graphite.

Like electrical conductivity, melt-state shear storage modulus (G') is a property that is highly sensitive to the formation a network-like structure in polymer nanocomposites [72]. Fig. 5 is a log–log plot of storage modulus as a function of angular frequency. Samples include not only the PP-0.3G, PP-0.8G, PP-2.7G, and PP-8.4G processed under harsh SSSP conditions, but also two others: neat PP that had been subjected to harsh SSSP processing and a PP-2.7G sample processed under mild SSSP conditions. The SSSP-processed neat PP sample was used for rheological characterization to ensure impartial comparison with the SSSP-processed PP-G series because moderate chain scission of the polymer can occur during SSSP [73,74]. In particular, the SSSP-processed PP exhibited lower G' values than the original, non-processed pellet PP (e.g., G'(10 rad/s, 200 °C) = 25900 Pa for the non-processed PP vs. 8500 Pa for SSSP-processed PP).

Incorporating increasing amounts of graphite nanofillers substantially increases G', especially at low angular frequency. However, the most dramatic effect is observed when the graphite nanofiller content is increased from 0.8 to 2.7 wt% in the samples made by harsh SSSP processing. Not only is there a major increase in G' with this increase in graphite content, but the slopes of the

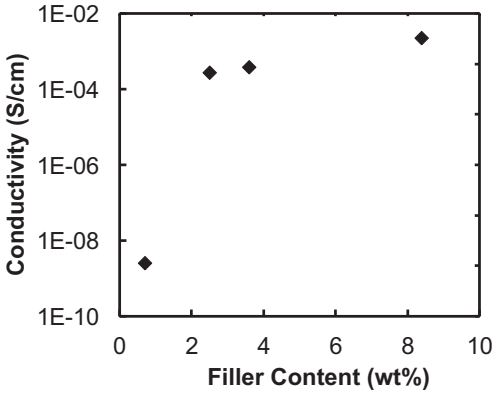

Fig. 4. Electrical conductivity of PP-graphite nanocomposites as a function of graphite content. Note that neat PP and PP-0.3G samples were found to be non-conductive and thus are not included in the plot.

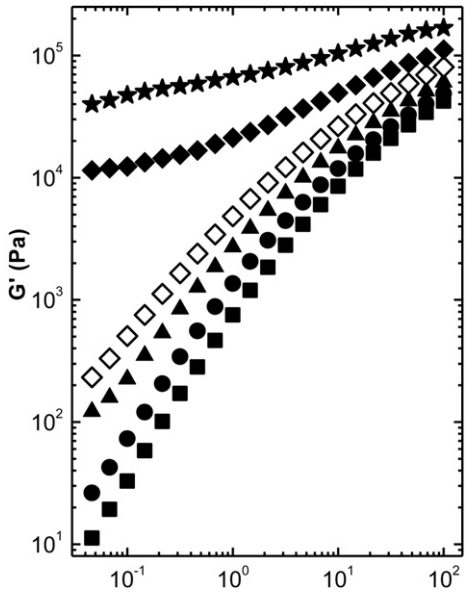

Fig. 5. Storage modulus as a function of angular frequency for a series of PP-graphite nanocomposites (at 200 °C): (◇) PP-2.7G via mild SSSP condition (1-pass); and (■) neat PP after SSSP, (●) PP-0.3G, (▲) PP-0.8G, (◆) PP-2.7G, and (★) PP-8.4G via harsh SSSP condition (5-pass).

curves at low frequency are very different. The neat PP, PP-0.3G and PP-0.8G curves all exhibit slopes of ~2 at low frequency, indicating that the nanocomposite melt behaves like a viscous liquid [75]. However, in the PP-2.7G and PP-8.4G samples made by harsh SSSP processing, the rheological response changes dramatically to an elastic solid-like behavior, with only a very limited reduction in G' with decreasing angular frequency. This elastic solid-like response is consistent with the development of a network-like structure associated with nanofiller. Thus, the rheological data are in accordance with the electrical conductivity data, indicating a percolation limit in the nanocomposites made by harsh SSSP conditions of between 0.8 and 2.7 wt% graphite.

Fig. 5 also compares G' values for the PP-2.7G nanocomposite as a function of SSSP processing. When subjected to mild SSSP processing, the PP-2.7G nanocomposite exhibits behavior that is only slightly more stiff than that of the PP-0.8G sample made by harsh SSSP processing and that is consistent with a viscous liquid rather than an elastic solid. This behavior indicates that the extent of SSSP processing plays a key role in the exfoliation and dispersion of the graphite nanofiller. In order to achieve a network-like structure of nanofiller throughout the 2.7 wt% graphite hybrid, the pulverization needs to be sufficiently harsh to yield high enough levels of exfoliation and dispersion.

3.4. Mechanical properties

Table 2 summarizes the effect of graphite content on mechanical properties of PP nanocomposites made by harsh SSSP processing. Relative to neat PP, addition of 0.3 wt% graphite results in a ~50% increase in Young's modulus and a ~45% increase in yield strength with little reduction in elongation at break or impact strength. Young's modulus and yield strength exhibit maximum values at 2.7 wt% graphite content, ~100% and ~60% above those of neat PP, respectively. Although the modulus and strength decrease with increasing graphite content above 2.7 wt%, they nevertheless remain well above those of neat PP even at 8.4 wt% graphite content. All nanocomposites maintain good ductility and high elongation at break values except the sample with the highest

Table 2
Mechanical Property Enhancements in PP-Graphite Nanocomposites.

Samples	Young's Modulus E (MPa)	Yield Strength σ_y (MPa)	Elongation at Break ε_B (%)	Impact Strength[a] W (J/cm)
Neat PP, Pellet	910 +/− 30	27 +/− 1	810 +/− 40	3.1 +/− 0.5
PP-0.3G	1360 +/− 250	39 +/− 2	690 +/− 100	2.4 +/− 0.5
PP-0.8G	1480 +/− 280	40 +/− 2	740 +/− 90	1.5 +/− 0.5
PP-2.7G	1830 +/− 140	43 +/− 2	560 +/− 60	1.2 +/− 0.2
PP-3.6G	1270 +/− 80	34 +/− 2	380 +/− 180	0.7 +/− 0.7
PP-8.4G	1370 +/− 70	33 +/− 3	15 +/− 4	0.6 +/− 0.7

[a] Measured as absorbed impact energy per thickness.

graphite content, PP-8.4G, which exhibits brittle behavior. Unsurprisingly, impact strength decreases substantially with increasing graphite content.

3.5. Exfoliation and dispersion – effects of properties and tunability by processing

A comparison of the thermal, electrical, rheological and mechanical properties of the nanocomposites made by SSSP indicate substantially different responses as a function of graphite content. Crystallization temperature and half-time and thermal stability change monotonically with graphite content, with the greatest effect obtained at very low nanofiller content. Electrical conductivity and rheological response also change monotonically with graphite content, but with the most dramatic change occurring at a graphite composition reflecting the percolation threshold. Like thermal properties, tensile modulus and strength also exhibit the most significant increases as low graphite content. But unlike thermal properties, electrical conductivity and rheological response, the tensile properties exhibit maxima at a composition of 2.7 wt% graphite. Thus, a number of different optimal graphite compositions are possible depending on the intended (multifunctional) use of the nanocomposites and the graphite exfoliation/dispersion levels achieved during processing. When high levels of exfoliation are achieved via SSSP [50] or chemical functionalization of graphite oxide [64], many of the resulting graphite nanoplatelets contain only a small number of individual graphene sheets, and therefore are less mechanically robust cross-plane compared to in-plane. Such nanoplatelets may not be embedded in the matrix in a fully extended sheet form, but rather in more wrinkled forms [39,50,60]. Such states of graphite nanoplatelets are not expected to provide optimum mechanical reinforcement [76], which may explain in part why the Young's modulus value at 2.7 wt% graphite loading is a factor of 3 below what is predicted by the upper bound of a micromechanical model for this composite with appropriate filler shape, content and orientation [42,50]. However, a part of this difference between experiment and model predictions is surely related to the extent of exfoliation in the nanocomposites, which, based on the XRD data shown in Fig. 1, is known to be substantial but imperfect in the 2.7 wt% graphite nanocomposite.

In order to address this issue further, we compared the effects of SSSP process conditions on the exfoliation levels achieved in selected PP-graphite nanocomposites and on several of their resulting properties. Fig. 6 compares XRD data for nanocomposites of identical graphite content, with normalization of data done identically to those shown in Fig. 1. The PP-2.7G samples were made by harsh SSSP processing and mild SSSP processing. The graphite XRD peak height is substantially reduced by harsh SSSP processing (by ~30% relative to the sample made by mild SSSP processing), indicating achievement of greater exfoliation. Consistent with this determination are the rheology data shown in Fig. 5, in which the G' data for the PP-2.7G sample made by mild SSSP processing are not only substantially below those for the PP-2.7G sample made by harsh SSSP processing, but also exhibit a liquid-like response rather than a solid-like response at low frequency. Thermal characterization results presented in Table 3 show that the $\tau_{1/2}$ reductions and T_{deg} enhancements are substantially greater in the harsh SSSP samples for both sets of graphite loadings (2.7 wt% and 3.6 wt%). Therefore, the degree of nanoplatelet exfoliation and the relevant property enhancements can be easily tuned by controlling the harshness of the SSSP process.

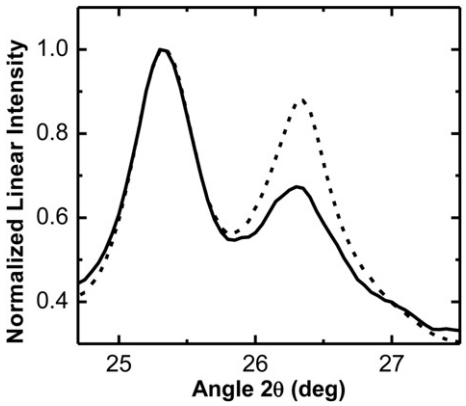

Fig. 6. X-ray diffraction of (—) PP-2.7G prepared by harsh SSSP processing and (– – –) PP-2.7G prepared by mild SSSP processing.

Lastly, our property characterization results draw attention to the independent nature of exfoliation and dispersion of graphite nanoplatelets in the polymer matrix. Previous work on PP-multiwall carbon nanotube composites has shown that the SSSP processing can partially debundle the nanotube aggregates, with subsequent melt mixing leading to further dispersion and debundling of the nanotubes [24]. In a preliminary experiment, a 3.6 wt% graphite nanocomposite was made by mild SSSP processing followed by melt mixing at 240 °C in a bench-top batch mixer. This combination of mild SSSP processing and melt mixing is adequate to promote faster crystallization kinetics ($\tau_{1/2}$ = 13 min at 148 °C) and higher degradation stability (T_{deg} = 448 °C) than those obtained in PP-3.6G sample made by harsh SSSP processing alone. We postulate that this even greater achievement of property enhancement by the two-step processing route is caused by partial exfoliation of the graphite nanoplatelets by mild SSSP, including the presence of agglomerates of graphite interpenetrated by PP, and subsequent relatively homogeneous distribution and dispersion of the exfoliated particles by the melt-mixing process. Further investigation is warranted and underway.

Table 3
Effect of Different Fabrication Methods upon the Thermal Properties for PP-Graphite Nanocomposites at Two Filler Loadings.

Samples	Fabrication Method	Actual Graphite Content w_{act} (wt%)	Thermal Degradation Temperature, at 5 wt% loss of total mass T_{deg} (°C)	Isothermal Crystallization Half-Time, at 148 °C $\tau_{1/2}$ (min)
PP-2.7G	SSSP, harsh (5-pass)	2.7	429	23
PP-2.7G-mild	SSSP, mild (1-pass)	2.7	420	42
PP-3.6G	SSSP, harsh (5-pass)	3.6	435	16
PP-3.6G-mild	SSSP, mild (1-pass)	3.6	422	31

Acknowledgements

We acknowledge support from Northwestern University, the NSF-MRSEC program (Grant DMR-0520513) at the Materials Research Center of Northwestern University, and Toray Industries for funding. We also thank Albert Tamashausky at Asbury Carbons for the supply of graphite and technical discussions. X-ray diffraction measurements were conducted at the J. B. Cohen X-ray Diffraction Facility and mechanical characterization was conducted at the Central Laboratory for Materials Mechanical Properties, both at Northwestern University.

References

[1] Usuki A, Kojima Y, Kawasumi M, Okada A, Fukushima Y, Kurauchi T, et al. J Mater Res 1993;8:1179–84.
[2] Giannelis EP. Adv Mater 1996;8:29–35.
[3] Alexandre M, Dubois P. Mater Sci Eng R 2000;28:1–63.
[4] Pavlidou S, Papaspyrides CD. Prog Polym Sci 2008;33:1119–98.
[5] Gunes IS, Cao F, Jana SC. Polymer 2008;49:2223–34.
[6] Paul DR, Robeson LM. Polymer 2008;49:3187–204.
[7] Al-Saleh MH, Sundararaj U. Polymer 2010;51:2740–7.
[8] Rittigstein P, Torkelson JM. J Polym Sci Part B Polym Phys 2006;44:2935–43.
[9] Rittigstein P, Priestley RD, Broadbelt LJ, Torkelson JM. Nat Mater 2007;6: 278–82.
[10] Kim JY, Il Han S, Hong SP. Polymer 2008;49:3334–45.
[11] Vaia RA, Giannelis EP. MRS Bull 2001;26:394–401.
[12] Cho JW, Paul DR. Polymer 2001;42:1083–94.
[13] Manias E, Touny A, Wu L, Strawhecker K, Lu B, Chung TC. Chem Mater 2001;13:3516–23.
[14] Gopakumar TG, Lee JA, Kontopoulou M, Parent JS. Polymer 2002;43:5483–91.
[15] Sheng N, Boyce MC, Parks DM, Rutledge GC, Abes JI, Cohen RE. Polymer 2004;45:487–506.
[16] Haggenmueller R, Gommans HH, Rinzler AG, Fischer JE, Winey KI. Chem Phys Lett 2000;330:219–25.
[17] Ajayan PM, Schadler LS, Giannaris C, Rubio A. Adv Mater 2000;12:750–3.
[18] Potschke P, Fornes TD, Paul DR. Polymer 2002;43:3247–55.
[19] Breuer O, Sundararaj U. Polym Composite 2004;25:630–45.
[20] McNally T, Potschke P, Halley P, Murphy M, Martin D, Bell SEJ, et al. Polymer 2005;46:8222–32.
[21] Ramanathan T, Liu H, Brinson LC. J Polym Sci Part B Polym Phys 2005;43:2269–79.
[22] Moniruzzaman M, Winey KI. Macromolecules 2006;39:5194–205.
[23] Villmow T, Potschke P, Pegel S, Haussler L, Kretzchmar B. Polymer 2008;49: 3500–9.
[24] Masuda J, Torkelson JM. Macromolecules 2008;41:5974–7.
[25] Mu MF, Walker AM, Torkelson JM, Winey KI. Polymer 2008;49:1332–7.
[26] Pujari S, Ramanathan T, Kasimatis K, Masuda J, Andrews R, Torkelson JM, et al. J Polym Sci Part B Polym Phys 2009;47:1426–36.
[27] Isayev AI, Kumar R, Lewis TM. Polymer 2009;50:250–60.
[28] Chen LM, Ozisik R, Schadler LS. Polymer 2010;51:2368–75.
[29] Pan YX, Yu ZZ, Ou YC, Hu GH. J Polym Sci Part B Polym Phys 2000;38:1626–33.
[30] Chen GH, Wu DJ, Weng WG, Yan WL. J Appl Polym Sci 2001;82:2506–13.
[31] Xiao P, Xiao M, Gong KC. Polymer 2001;42:4813–6.
[32] Chen XM, Shen JW, Huang WY. J Mater Sci Lett 2002;21:213–4.
[33] Zheng WG, Wong SC, Sue HJ. Polymer 2002;43:6767–73.
[34] Du XS, Xiao M, Meng YZ. Eur Polym J 2004;40:1489–93.
[35] Gopakumar TG, Page DJYS. Polym Eng Sci 2004;44:1162–9.
[36] Mack JJ, Viculis LM, Ali A, Luoh R, Yang GL, Hahn HT, et al. Adv Mater 2005;17:77–80.
[37] Uhl FM, Yao Q, Nakajima H, Manias E, Wilkie CA. Polym Degrad Stab 2005;89:70–84.
[38] Yasmin A, Luo JJ, Daniel IM. Compos Sci Technol 2006;66:1182–9.
[39] Stankovich S, Dikin DA, Dommett GHB, Kohlhaas KM, Zimney EJ, Stach EA, et al. Nature 2006;442:282–6.
[40] Debelak B, Lafdi K. Carbon 2007;45:1727–34.
[41] Li J, Kim JK. Compos Sci Technol 2007;67:2114–20.
[42] Ramanathan T, Stankovich S, Dikin DA, Liu H, Shen H, Nguyen ST, et al. J Polym Sci Part B Polym Phys 2007;45:2097–112.
[43] Kalaitzidou K, Fukushima H, Drzal LT. Carbon 2007;45:1446–52.
[44] Verdejo R, Barroso-Bujans F, Rodriguez-Perez MA, de Saja JA, Lopez-Manchado MA. J Mater Chem 2008;18:2221–6.
[45] Bourdo S, Li ZR, Biris AS, Watanabe F, Viswanathan T, Pavel I. Adv Funct Mater 2008;18:432–40.
[46] Kalaitzidou K, Fukushima H, Askeland P, Drzal LT. J Mater Sci 2008;43: 2895–907.
[47] Kim H, Macosko CW. Macromolecules 2008;41:3317–27.
[48] Otieno G, Kim JY. Ind Eng Chem 2008;14:187–93.
[49] Ramanathan T, Abdala AA, Stankovich S, Dikin DA, Herrera-Alonso M, Piner RD, et al. Nat Nanotechnol 2008;3:327–31.
[50] Wakabayashi K, Pierre C, Dikin DA, Ruoff RS, Ramanathan T, Brinson LC, et al. Macromolecules 2008;41:1905–8.
[51] Steurer P, Wissert R, Thomann R, Mulhaupt R. Macromol Rapid Commun 2009;30:316–27.
[52] Vickery JL, Patil AJ, Mann S. Adv Mater 2009;21:2180–4.
[53] Kim H, Macosko CW. Polymer 2009;50:3797–809.
[54] Ansari S, Giannelis EP. J Polym Sci Part B Polym Phys 2009;47:888–97.
[55] Potschke P, Abdel-Goad M, Pegel S, Jehnichen D, Mark JE, Zhou DH, et al. Macromol Sci A Pure Appl Chem 2010;47:12–9.
[56] Ober CK, Cheng SZD, Hammond PT, Muthukumar M, Reichmanis E, Wooley KL, et al. Macromolecules 2009;42:465–71.
[57] Kelly BT. Physics of graphite. London: Applied Science Publishers; 1981.
[58] Chung DDL. J Mater Sci 2002;37:1475–89.
[59] Geim AK, Novoselov KS. Nat Mater 2007;6:183–91.
[60] Stankovich S, Dikin DA, Piner RD, Kohlhaas KA, Kleinhammes A, Jia Y, et al. Carbon 2007;45:1558–65.
[61] van den Brink J. Nat Nanotechnol 2007;2:199–201.
[62] Schniepp HC, Li JL, McAllister MJ, Sai H, Herrera-Alonso M, Adamson DH, et al. J Phys Chem B 2006;110:8535–9.
[63] Li D, Kaner RB. Science 2008;320:1170–1.
[64] Balandin AA, Ghosh S, Bao WZ, Calizo I, Teweldebrhan D, Miao F, et al. Nano Lett 2008;8:902–7.
[65] Compton OC, Nguyen ST. Small 2010;6:711–23.
[66] Furgiuele N, Lebovitz AH, Khait K, Torkelson JM. Macromolecules 2000;33: 225–8.
[67] Lebovitz AH, Khait K, Torkelson JM. Macromolecules 2002;35:8672–5.
[68] Tao Y, Kim J, Torkelson JM. Polymer 2006;47:6773–81.
[69] Kasimatis K, Torkelson JM. PMSE Prepr 2004;91:173–4.
[70] Khait K, Torkelson JM. Polym-Plast Technol 1999;38:445–57.
[71] Bu HS, Cheng SZD, Wunderlich B. Makromol Chem Rapid Commun 1988;9: 75–7.
[72] Xu L, Nakajima H, Manias E, Krishnamoorti R. Macromolecules 2009;42: 3795–803.
[73] Lebovitz AH, Khait K, Torkelson JM. Macromolecules 2002;35:9716–22.
[74] Ganglani M, Torkelson JM, Carr SH, Khait K. J Appl Polym Sci 2001;80:671–9.
[75] Ferry JD. Viscoelastic properties of polymers. 3rd ed. New York: Wiley; 1980.
[76] Fisher FT, Bradshaw RD, Brinson LC. Appl Phys Lett 2002;80:4647–9.